Efficient STATCOM based on hybrid sliding mode control-proportional integral control and 48-pulse converter

Hassen BELILA[1], Nasserdine BOUDJERDA[2], Ahsene BOUBAKIR[3], Imen BAHRI[4]
University of Oum El Bouaghi, Algeria (1), LER laboratory University of Jijel, Algeria (2), LAJ laboratory University of Jijel, Algeria (3), University of Paris-Saclay, France (4)

Abstract. *Flexible alternating current transmission systems (FACTS) evolved as a result of the development of power electronics and began to play a key role in improving the quality of Network power. The purpose of this work is to provide a control strategy of voltage and reactive power flow in one of the most used FACTS devices known as STATCOM. This strategy is based on a hybrid control (sliding mode control-classic PI control), in addition STATCOM uses a 48-pulse converter. The simulations proved the efficiency of the proposed system in both the control performance and harmonic distortion rate of the current injected into the grid.*

Keywords: STATCOM, Sliding Mode Control, reactive power compensation, 48-pulse converter, harmonics.

1. Introduction

The consumption of electrical energy is continually increasing as a result of industrialization and population increase. Thus, in order to achieve a balance between production and consumption, the number of power stations, lines, transformers, and other equipments in the power network must be increased, resulting in higher costs and environmental degradation [1].

The traditional means of electricity generation (thermal and nuclear power stations) are well adapted to the performance of electrical systems because their production is controllable, however, they use energy ressources with significant environmental disadvantages: Limited reserves, greenhouse gas emissions, and waste disposal, (particularly nuclear waste) [1], [2]. These energy and environmental concerns have pushed the evolution of electrical networks toward a vast integration of new unconventional and distributed electricity production sources, (particularly wind and photovoltaics PV), characterized by their reliance on climatic conditions (wind for aeolian and sunlight for PV) [2].

The current needs of consumers for high quality electricity require a highly efficient network. Many customers may be faced with major technical and economic problems as a result of poor energy quality due to the increasing sensitivity of the receivers and the process controls used. Disturbances such as voltage fluctuations, flashing, harmonics, or imbalances can prohibit devices from functioning properly and force certain industrial processes to shut down [3]–[7].

Conventional network control means such as electromechanical devices (transformer with adjustable load supports, phase-shifting transformers, serial or parallel compensators switched by circuit breakers, modification of production instructions, change in network topology, and action on generator excitation) may prove to be too slow and insufficient in the future to respond effectively to network disturbances, especially given the new constraints.

The rapid development of power electronics has given a significant impact on improving power grid operation by improving parameter control and introducing control devices based on advanced power electronics (GTO, IGBT), known as FACTS (Flexible Alternative Current Transmission Systems) [8].

The latest generation of FACTS systems is mostly composed of voltage (or current) converters based on modern static switches (GTO, IGBT), connected to capacitors as continuous voltage sources. These converters can be classified based on their network connection as shunt, series, or hybrid compensators, such as STATCOM (STATic COMpensator), SSSC (Static Synchronous Series Compensator), and UPFC (Unified Power Flow Controller) respectively.

The STATCOM is commonly used for reactive energy compensation and, as a result, voltage regulation at the bus bar to which it is linked. It generates a three-phase AC voltage synchronized with the voltage of the electrical grid from a DC voltage source. In practice, no active power is involved; only reactive power is exchanged between the STATCOM and the power grid, allowing for both power factor correction and compensation for falls and surges, hence enhancing the power quality of the network [8]–[10].

Extensive studies in recent years have revealed that the success of STATCOM is heavily dependent on the accuracy and robustness of the adopted control approach [11], [12].

Traditional PI controllers are generally simple to implement, however they are heavily affected by parameter variations and may suffer from stability issues; as a result, the authors of the reference [13] present an adaptive PI control of a STATCOM. In [14] and [15], the authors suggest a fuzzy logic control of a D-STATCOM (D-STATCOM: STATCOM coupled to a low voltage distribution network) and the results are compared with those of a standard PI control. However, it should be mentioned that this new technique has a long response time and a noisy stationary state (small oscillations). The authors of reference [16] used a D-STATCOM to adjust the output voltage of a hybrid power plant (eolian-diesel unit), and a sliding mode control was used. The authors of reference [17] attempt to improve the performance of a D-STATCOM connected to a low-voltage distribution network by selecting an appropriate DC-side reference of the D-STATCOM, this method reduces switching losses and current harmonics of the D-STATCOM without degrading its dynamics, a conventional PI control was used. The authors of reference [18] proposed a hybrid approach (SMC-PI) on a D-STATCOM to increase both static and dynamic performance over the usual PI configuration.

In the present work, we investigate the compensation of high voltage transmission lines by using a STATCOM system. Knowing that the control strategy is critical for good static and dynamic performance, we suggest a hybrid control method (sliding mode control–PI control) as we know the robustness and the dynamic performance of the sliding mode technique in general. In addition, we propose the use of a 48-pulse converter as an inverter for the STATCOM topology given its very low rate of harmonic distortion on the AC side.

2. Modeling of the grid connected STATCOM

The equivalent diagram of the STATCOM can be found in (Fig.1). Only the busbar of the common coupling point (CCP) is considered for the STATCOM modeling and the DC source is assumed to be constant (Fig.1.a). As a result, the equivalent circuit of Fig.1.b is an AC voltage source v_{sh} coupled to a

network node by the inductor L_{sh} of a coupling transformer and a resistor R_{sh} representing the transformer's ohmic losses and the inverter's switching losses [19]. The current i_{sh} is determined by the difference between the node voltage v_r and the STATCOM's adjustable voltage v_{sh} [20][21].

The amount of reactive power transferred between the STATCOM and the network is managed by the amplitude of the STATCOM voltage v_{sh}. This reactive energy is either injected into or removed from the network, allowing the bus bar voltage v_r to be regulated at a desired value [22].

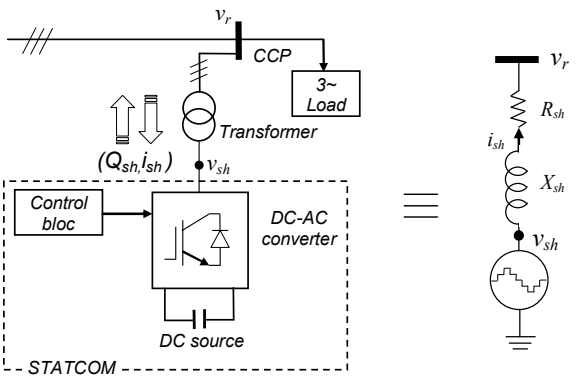

a. Bloc diagram b. Equivalent circuit

Fig.1. Equivalent diagram of a STATCOM

The application of Kirchhoff's laws on the equivalent circuit of Fig.1.b gives:

$$\begin{cases} v_{sha} - v_{ra} = R_{sh} i_{sha} + L_{sh} \dfrac{di_{sha}}{dt} \\ v_{shb} - v_{rb} = R_{sh} i_{shb} + L_{sh} \dfrac{di_{shb}}{dt} \\ v_{shc} - v_{rc} = R_{sh} i_{shc} + L_{sh} \dfrac{di_{shc}}{dt} \end{cases} \quad (1)$$

Where:

(v_{ra} , v_{rb} , v_{rc}): Three phase voltages at the CCP.

(v_{sha} , v_{shb} , v_{shc}): Three phase voltages at the output of the STATCOM.

(i_{sha} , i_{shb} , i_{shc}): Three phase shunt current of the STATCOM.

The well-known Park transformation allows the following transition from a balanced three phase system (a, b, c) to a rotating frame with only two orthogonal axes (d,q) [27]:

$$\begin{bmatrix} x_d \\ x_q \end{bmatrix} = P(\theta) \begin{bmatrix} x_a \\ x_b \\ x \end{bmatrix} \quad (2)$$

Where:

(x_a,x_b,x_c): Phase components of the three phase system (voltage, current …).

(x_d,x_q) : Park components.

θ : Angle between the phase axis *a* and the rotating axis *d*.

$P(\theta)$: Transformation matrix given as follow:

$$[P(\theta)] = \sqrt{\frac{2}{3}} \begin{bmatrix} \cos(\theta) & \cos(\theta - 2\pi/3) & \cos(\theta + 2\pi/3) \\ \sin(\theta) & \sin(\theta - 2\pi/3) & \sin(\theta + 2\pi/3) \end{bmatrix}$$

The inverse Park transformation allows the return to phase components (*a*, *b*, *c*) as follows:

$$\begin{bmatrix} x_a \\ x_b \\ x_c \end{bmatrix} = P(\theta)^{-1} . \begin{bmatrix} x_d \\ x_q \end{bmatrix} \quad (3)$$

$P(\theta)^{-1}$: Inverse transformation matrix.

Considering $\theta = 2\pi ft$ (f : frequency of the grid currents), the application of park transformation to equation (1) gives [23]:

$$\begin{cases} v_{shd} - v_{rd} = R_{sh} i_{shd} + L_{sh} \dfrac{di_{shd}}{dt} - \omega L_{sh} i_{shq} \\ v_{shq} - v_{rq} = R_{sh} i_{shq} + L_{sh} \dfrac{di_{shq}}{dt} + \omega L_{sh} i_{shd} \end{cases} \quad (4)$$

Then, we can write the following state equation of the STATCOM:

$$\begin{cases} \dot{x}_1 = \dfrac{d}{dt} i_{shd} = -\dfrac{R_{sh}}{L_{sh}} i_{shd} + \omega . i_{shq} - \dfrac{1}{L_{sh}} v_{rd} + \dfrac{1}{L_{sh}} u_1 \\ \dot{x}_2 = \dfrac{d}{dt} i_{shq} = -\dfrac{R_{sh}}{L_{sh}} i_{shq} - \omega . i_{shd} - \dfrac{1}{L_{sh}} v_{rq} + \dfrac{1}{L_{sh}} u_2 \end{cases} \quad (5)$$

Where:

$\begin{bmatrix} u_1 \\ u_2 \end{bmatrix} = \begin{bmatrix} v_{shd} \\ v_{shq} \end{bmatrix}$: Input vector of the system.

$\begin{bmatrix} x_1 \\ x_2 \end{bmatrix} = \begin{bmatrix} i_{shd} \\ i_{shq} \end{bmatrix}$: State variables of the system.

3. Proposed sliding mode control of the STATCOM

According to equation (5), the relative degrees of outputs $x_1 = i_{shd}$ and $x_2 = i_{shq}$ are unit, i.e. $r_1 = r_2 = 1$. To boost pursuit performance in steady state we picked the following integral type sliding surfaces [24]:

$$S_1 = \left(\frac{d}{dt} + \lambda_1 \right) \int_0^t e_1 \quad (6)$$

And,

$$S_2 = \left(\frac{d}{dt} + \lambda_2 \right) \int_0^t e_2 \quad (7)$$

Where:

$$e_1 = i_{shd}^* - i_{shd} \quad (8)$$

And,

$$e_2 = i_{shq}^* - i_{shq} \quad (9)$$

By inserting equations (8) and (9) into (6) and (7), respectively, we obtain the derivatives of the following sliding surfaces:

$$\dot{S}_1 = \dot{i}_{shq}^* - \dot{i}_{shq} + \lambda_1 . e_1 \quad (10)$$

And,

$$\dot{S}_2 = \dot{i}_{shq}^* - \dot{i}_{shq} + \lambda_2 . e_2 \quad (11)$$

Then, by inserting equations (5) into (10) and (11), we get:

$$\dot{S}_1 = \dot{i}^*_{shd} + \frac{R_{sh}}{L_{sh}} i_{shd} - \omega . i_{shq} + \frac{1}{L_{sh}} v_{rd} - \frac{1}{L_{sh}} u_1 + \lambda_1 . e_1 \quad (12)$$

And,

$$\dot{S}_2 = \dot{i}^*_{shq} + \frac{R_{sh}}{L_{sh}} i_{shq} + \omega . i_{shd} + \frac{1}{L_{sh}} v_{rq} - \frac{1}{L_{sh}} u_2 + \lambda_2 . e_2 \quad (13)$$

And, in order to check Lyapounov's stability criterion ($S_i . \dot{S}_i < 0$), we must have:

$$\dot{S}_1 = -\alpha_1 S_1 - \beta_1 \, sign(S_1) \quad (14)$$

And,

$$\dot{S}_2 = -\alpha_2 S_2 - \beta_2 sign(S_2) \quad (15)$$

Where α_1 , α_2 , β_1 , β_2 are design parameters chosen based on desired closed loop performance. They enable the designer to increase response speed and robustness vis-à-vis uncertainties and exogenous inputs.

Note: The greater and larger the numbers α_1 and α_2 , the faster the time of attractiveness towards the sliding surface; while low values β_1 and β_2 lower the oscillations.

By equating equations (12) with (14) and (13) with (15), we get:

$$\dot{i}^*_{shd} + \frac{R_{sh}}{L_{sh}} i_{shd} - \omega . i_{shq} + \frac{1}{L_{sh}} v_{rd} - \frac{1}{L_{sh}} u_1 + \lambda_1 . e_1 = -\alpha_1 S_1 - \beta_1 \, sign(S_1) \quad (16)$$

And,

$$\dot{i}^*_{shq} + \frac{R_{sh}}{L_{sh}} i_{shq} + \omega . i_{shd} + \frac{1}{L_{sh}} v_{rq} - \frac{1}{L_{sh}} u_2 + \lambda_2 . e_2 = -\alpha_2 S_2 - \beta_2 sign(S_2) \quad (17)$$

This allows us to find the following u_1 and u_2 command expressions:

$$u_1 = L_{sh} \dot{i}^*_{shd} + R_{sh} i_{shd} - L_{sh} \omega . i_{shq} + v_{rd} + L_{sh} \lambda_1 e_1 + \alpha_1 L_{sh} S_1 + \beta_1 L_{sh} \, sign(S_1) \quad (18)$$

And,

$$u_2 = L_{sh} \dot{i}^*_{shq} + R_{sh} i_{shq} + L_{sh} \omega . i_{shd} + v_{rq} + L_{sh} \lambda_2 e_2 + \alpha_2 L_{sh} S_2 + \beta_2 L_{sh} \, sign(S_2) \quad (19)$$

Taking into consideration:

$$u_1 = u_{eq1} + u_{c1} \quad (20)$$

And,

$$u_2 = u_{eq2} + u_{c2} \quad (21)$$

Finally, the following formula defines the command:

- The terms of the u_{eq1} and u_{eq2} equivalent commands, specified as follows:

$$u_{eq1} = L_{sh} \dot{i}^*_{shd} + R_{sh} i_{shd} - L_{sh} \omega . i_{shq} + v_{rd} + L_{sh} \lambda_1 e_1 \quad (22)$$

And,

$$u_{eq2} = L_{sh} \dot{i}^*_{shq} + R_{sh} i_{shq} + L_{sh} \omega . i_{shd} + v_{rq} + L_{sh} \lambda_2 e_2 \quad (23)$$

- Correction terms u_{c1} and u_{c2} :

$$u_{c1} = \alpha_1 L_{sh} S_1 + \beta_1 L_{sh} \, sign(S_1) \quad (24)$$

And,

$$u_{c2} = \alpha_2 L_{sh} S_2 + \beta_2 L_{sh} \, sign(S_2) \quad (25)$$

Finally, we propose in Figure 2, the bloc diagram of the hybrid SMC-PI strategy of the STATCOM based on an internal SMC control of two variables (i_{sd} and i_{sa}) and two external PI control loops for V_{dc} and v_r . This control strategy can be explained as follows:

- The two internal current control loops are achieved by a STATCOM-SMC control block.
- The continuous bus voltage control loop's role is to keep this voltage constant by controlling the active power transit between the PCC and the continuous bus. The reference voltage V^*_{dc} and measured voltage V_{dc} are the regulator's inputs, and the output is the direct component of the reference current i^*_{shd} (Fig. 2). This voltage is frequently controlled by a PI type regulator [25].
- The control of the reactive power exchange between the STATCOM and the power grid regulates the v_r voltage at the 'PCC' coupling point. As shown in Figure 2, a PI controller generates a reference signal for the STATCOM's reactive current component i^*_{shq} .

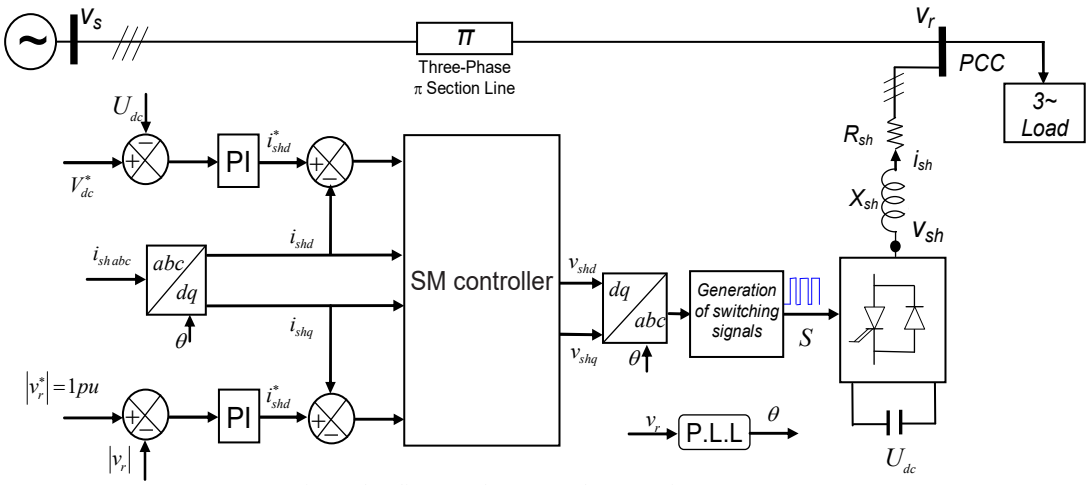

Fig.2. Bloc diagram of SM control strategy for STATCOM [24]

Because of its very low harmonic distortion content on the AC side, the 48-pulse converter can be used in high voltage and high power applications without the requirement for AC filters. This converter's consists of four identical three-level GTO converters (each requiring 12 control pulses) coupled together by four phase-shifting transformers, as shown in Figure 3 [26]. Transformers are specifically required in our application to raise the output voltage and adapt it to that of the network; they thus serve a dual purpose: they perform the phase shifts required to get multi-level voltage and they raise the voltage to match the very high voltage. In order to avoid very large number of switching operation, we use full-wave control which leeds to a minimum switching losses.

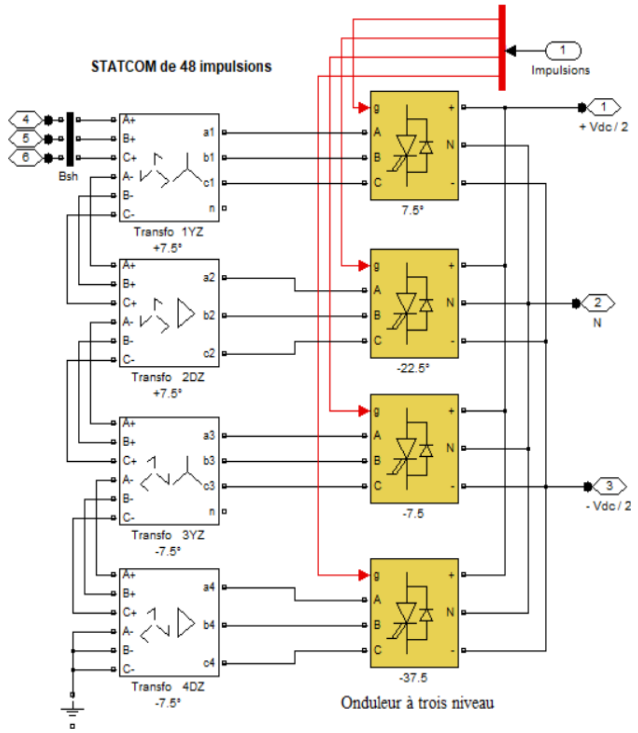

Fig.3. 48 pulse GTO voltage inverter

4. Simulations and results analysis

4.1. Simulations

Figure 4 presents a single-line diagram of the power network used to validate the operation of the proposed STATCOM.

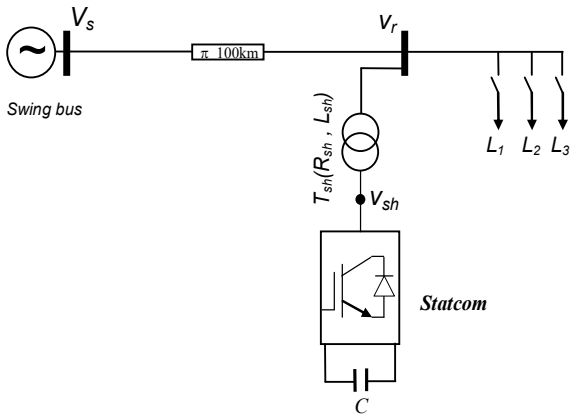

Fig.4. Single-line diagram of the studied network

The considered network is composed of a 400 KV reference generator and a transmission line modeled in π to supply a load (L1, L2, L3) at the set of bar '*r*'.
The T_{sh} transformer is used to reduce the voltage from 400 KV (network voltage) to 20 KV (STATCOM output voltage).

The simulations are carried out in a per unit system with base values of S_B = 1000 MVA and U_B = 400 kV, and the voltage of the generator busbar is V_S = 1.0 pu.
Three loads (L1, L2 and L3) are connected to the busbar " *r* " as shown in the following table:

Table 1. Load variation

Connection time(s)	0s to 0.5s	0.5 to 1s	1s to 1.5s	1.5s to 2s
Load	L1	L1+L2	L+L2+L3	L3

Where:
L1: inductive load , P1 = 1.0 pu and Q1 = 0.4 pu.
L2: inductive load , P2 = 0.5 pu, and Q2 = 0.4 pu.
L3: capacitive load , P3 = 0.3 pu, Q3c = 0.2 pu, Q3l = 0.01 pu

4.2. Results analysis

4.2.1 Network without STATCOM (STATCOM deconnected)

The voltage drop generated by the inductive load L2 at time t = 0.5 s is shown in Fig.5 at both the source and load bus bars V_s and V_r. At time t = 1 s, the capacitive load connection L3 naturally dampens this voltage drop. Finally, the disconnection of all inductive loads in the final transition at time t = 1.5 s resulted in a capacitive load flow and a surge at the two bus bars. Note t small influence of load fluctuations on the source bus bar.

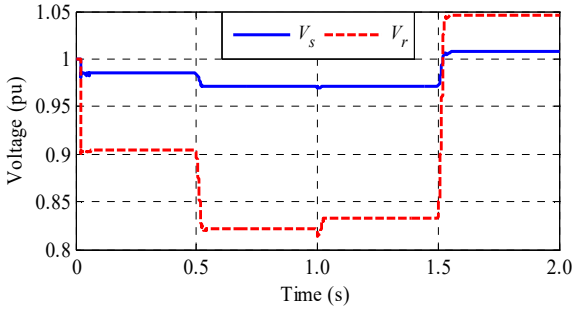

Fig.5. Source voltage v_s and load voltage v_r before compensation

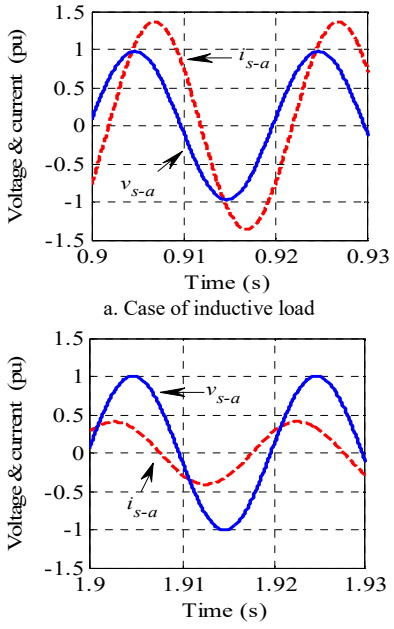

a. Case of inductive load

b. Case of capacitive load

Fig.6. Grid voltage v_s and current i_s before compensation

The phase shift between the voltage and current of the source is shown in Fig.6, and it is evident that the voltage is ahead of the current, as shown in Fig.6.a in the case of inductive load. In the

case of a capacitive load, the current is ahead of the voltage, as shown in Fig.6.b.

4.2.2. Network with connected STATCOM

The STATCOM produces reactive current (i_{shq}>0) for inductive loads and absorbs reactive current (i_{shq}<0) for capacitive loads, as shown in Fig.7.

In inductive mode the STATCOM injects a quantity of reactive power $Q_{sh} \approx$ [0.45 0.91 0.76] pu in the three intervals to raise the voltage v_r to 1.0 pu, while in capacitive mode the STATCOM absorbs reactive energy from the network(Q_{sh}<0) to keep the voltage profile v_r constant, as shown in Fig.8.
We notice that the STATCOM consumes a very low amount of active power to compensate for losses in the power switches of the static converter (Fig.8).

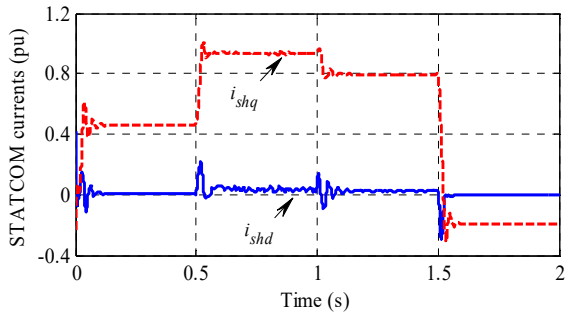

Fig.7. STATCOM currents i_{shd} and i_{shq}

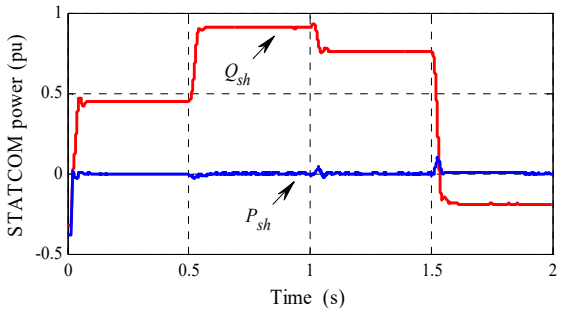

Fig.8. STATCOM Active and reactive power (P_{sh},Q_{sh})

The voltage of the load bus bar is well regulated at its nominal value, v_r = 1.0 pu, as shown in Fig.9. Furthermore, a favorable effect is also observed on the voltage v_s, which approaches its nominal value (Fig.9).

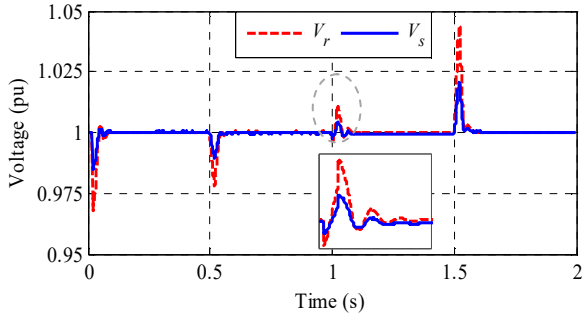

Fig.9. Source voltage v_s and load voltage v_r after SMC compensation

Figure 10 shows that the voltage v_s and the current i_s are in phase in steady state after compensation; indicating that there is no transit of reactive power between the source and the load after compensation.
Figure 11 displays the shapes and phase shift between the v_{sh} and v_r voltages after PI-SMC compensation; we note a zero phase shift (v_{sha} and v_{ra} are in phase). We can determine the capacitive mode of operation for (v_r < v_{sh}) and the inductive mode of operation for (v_r > v_{sh}). Furthermore, Fig.12 shows that i_{sh} current is forward quadrature to v_{sh} voltage for the capacitive mode and backward quadrature for the inductive mode, implying that only reactive energy is transferred between the STATCOM and the network. We notice the specific waveform of the output voltage of the 48-pulse converter which is very close to the sine wave.

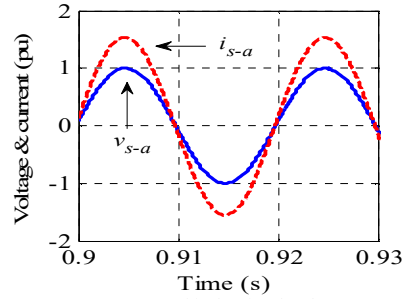

a. Case of inductive load

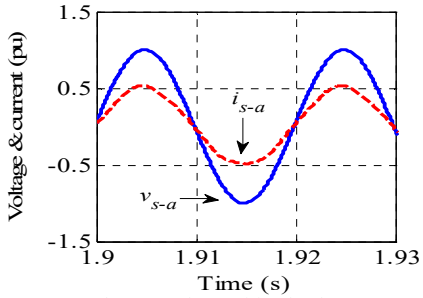

b. Case of capacitive load

Fig.10. Grid voltage v_s and current i_s after compensation

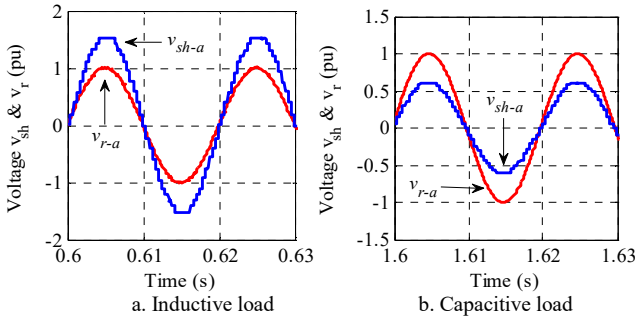

a. Inductive load b. Capacitive load

Fig.11. Grid voltage v_{sh-a} and v_{r-a} after compensation

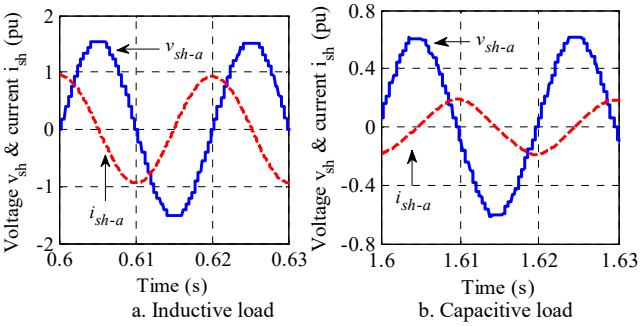

a. Inductive load b. Capacitive load

Fig.12. Grid voltage v_{sh-a} and current i_{sh-a} after compensation

Figure 13 shows the THD of v_{sh} voltage at the STATCOM output as well as the i_{sh} current injected into the network by the PI-SMC hybrid control. THD for voltage is 4.11 % and 0.90 % for current. These values are fully compliant with IEEE regulations, which focus only on the injected current by limiting its THD to 5% and the amplitude of each current harmonic to 3% [27].

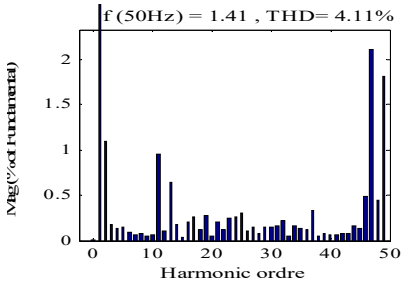

a. Harmonic spectrum of the $v_{sh\text{-}a}$

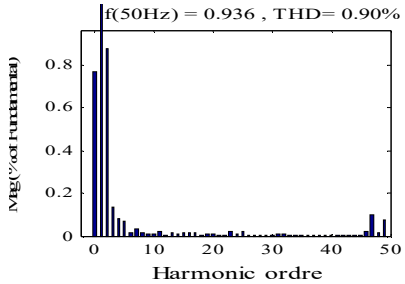

b. Harmonic spectrum of the $i_{sh\text{-}a}$

Fig. 13. Harmonic spectrum of the phase voltage $v_{sh\text{-}a}$ and current $i_{sh\text{-}a}$ at the STATCOM output

6. Conclusion

We began this paper by emphasizing the detrimental effect of reactive power transit on the load bus bar. Then we connected a STATCOM to this bar in order to adjust for reactive power and keep the voltage at its nominal value. In terms of compensation and enhanced energy quality, the adoption of hybrid control strategy (PI – SMC) has produced extremely excellent results. Indeed, the proposed innovative methodology ensures a very fast dynamic adjustment in the case of a rapid change in load and operates as a shock absorber, in addition to a better energy quality in a constant state. In addition the use of 48-pulse converter achieves an output voltage with very good shape while minimising the switching losses.

References

[1] B. Wu, Y. Lang, N. Zargari, and S. Kouro, "Power conversion and predictive control of wind energy conversion systems," in *John Wiley and sons Publication, IEEE Press*, 2011, p. 453.

[2] H. Bayem, "Apport des méthodes probabilistes aux études d ' intégration des énergies renouvelables aux systèmes électriques," Thèse de doctorat, Université Paris Sud - Paris XI, 2009.

[3] M. Moghbel, M. A. S. Masoum, A. Fereidouni, and S. Deilami, "Optimal sizing, siting and operation of custom power devices with STATCOM and APLC functions for real-time reactive power and network voltage quality control of smart grid," *IEEE Trans. Smart Grid*, vol. 9, no. 6, pp. 5564–5575, 2018, doi: 10.1109/TSG.2017.2690681.

[4] R. Moghe, D. Divan, D. Lewis, and J. Schatz, "Turning Distribution Feeders into STATCOMs," *IEEE Trans. Ind. Appl.*, vol. 53, no. 2, pp. 1372–1380, 2017, doi: 10.1109/TIA.2016.2634520.

[5] E. Kontos, G. Tsolaridis, R. Teodorescu, and P. Bauer, "High Order Voltage and Current Harmonic Mitigation Using the Modular Multilevel Converter STATCOM," *IEEE Access*, vol. 5, pp. 16684–16692, 2017, doi: 10.1109/ACCESS.2017.2749119.

[6] K. R. Padiyar, "Facts Controllers in Power Transmission Distribution," in *New age international publishers*, 2007, p. 548.

[7] L. Feola, R. Langella, I. Papic, and A. Testa, "Selective interharmonic compensation to improve statcom performance for light flicker mitigation," *IEEE Trans. Power Deliv.*, vol. 33, no. 5, pp. 2442–2451, 2018, doi: 10.1109/TPWRD.2018.2810333.

[8] K. K. Sen and M. L. Sen, "Introduction to FACTS Controllers: Theory, Modeling, and Applications," in *Wiley-IEEE Press*, 2009, p. 552.

[9] S. D. Mahajan, M. Murali, and T. B. Mali, "Comparative analysis of 6, 12 and 48 pulse T-STATCOM," *IEEE 7th Power India Int. Conf. PIICON*, 2016, doi: 10.1109/POWERI.2016.8077252.

[10] M. I. Mosaad, "Model reference adaptive control of STATCOM for grid integration of wind energy systems," *IET Electr. Power Appl.*, vol. 12, no. 5, pp. 605–613, 2018, doi: 10.1049/iet-epa.2017.0662.

[11] E. Tremblay, S. Atayde, and A. Chandra, "Comparative study of control strategies for the doubly fed induction generator in wind energy conversion systems: A DSP-based implementation approach," *IEEE Trans. Sustain. Energy*, vol. 2, no. 3, pp. 288–299, 2011, doi: 10.1109/TSTE.2011.2113381.

[12] G. Abad, J. Lopez, M. Rodriguez, L. Marroyo, and G. Iwanski, "Doubly Fed Induction Machine: Modeling and Control for Wind Energy Generation," in *Wiley-IEEE Press*, 2011, p. 625.

[13] Y. Xu and F. Li, "Adaptive PI control of STATCOM for voltage regulation," *IEEE Trans. Power Deliv.*, vol. 29, no. 3, pp. 1002–1011, 2014, doi: 10.1109/TPWRD.2013.2291576.

[14] S. K. Routray, N. Nayak, and P. K. Rout, "A Robust Fuzzy Sliding Mode Control Design for Current Source Inverter based STATCOM Application," *Procedia Technol.*, vol. 4, pp. 342–349, 2012, doi: 10.1016/j.protcy.2012.05.052.

[15] A. Ajami and N. Taheri, "A Hybrid Fuzzy/LQR Based Oscillation Damping Controller Using 3-level STATCOM," *Int. J. Comput. Electr. Eng.*, vol. 3, no. 2, pp. 184–189, 2011, doi: 10.7763/ijcee.2011.v3.312.

[16] H. Yunhao, S. Yuanyuan, Z. Han, and M. Yang, "Sliding mode reactive power control of isolated wind-disel hybrid power system based on STATCOM," *37th Chinese Control Conf. Jul. 2018, Wuhan, China*, pp. 8709–8714, 2018.

[17] S. Ziaeinejad and A. Mehrizi-Sani, "Design tradeoffs in selection of the DC-side voltage for a D-STATCOM," *IEEE Trans. Power Deliv.*, vol. 33, no. 6, pp. 3230–3232, 2018, doi: 10.1109/TPWRD.2017.2750422.

[18] F. Hamoud, M. L. Doumbia, and A. Cheriti, "Hybrid PI-Sliding Mode Control of a voltage source converter based STATCOM," *16th Int. Power Electron. Motion Control Conf. Expo. PEMC 2014*, pp. 661–666, 2014, doi: 10.1109/EPEPEMC.2014.6980571.

[19] S. K. Routray, N. Nayak, and P. K. Rout, "A Robust Fuzzy Sliding Mode Control Design for Current Source Inverter based STATCOM Application," *Procedia Technol.*, vol. 4, pp. 342–349, 2012, doi: 10.1016/j.protcy.2012.05.052.

[20] S. Gerbex, R. Cherkaoui, and A. J. Germond, "Optimal location of multi-type FACTS devices in a power system by means of genetic algorithms," *IEEE Trans. Power Syst.*, vol. 16, no. 3, pp. 537–544, 2001, doi: 10.1109/59.932292.

[21] N. Yorino, E. E. El-Araby, H. Sasaki, and S. Harada, "A new formulation for FACTS allocation for security enhancement against voltage collapse," *IEEE Trans. Power Syst.*, vol. 18, no. 1, pp. 3–10, 2003, doi: 10.1109/TPWRS.2002.804921.

[22] F. Shahnia, S. Rajakaruna, and A. Ghosh, "Static Compensators (STATCOMs) in Power Systems," in *Power Systems*, 2015.

[23] S. A. Touil, N. Boudjerda, A. Boubakir, and K. El Khamlichi Drissi, "A sliding mode control and artificial neural network based MPPT for a direct grid-connected photovoltaic source," *Asian J. Control*, vol. 21, no. 4, pp. 1892–1905, 2019, doi: 10.1002/asjc.2007.

[24] H. Belila, N. Boudjerda, A. BOUBAKIR, and I. BAHRI, "Improved STATCOM efficiency using a hybrid technique based on sliding mode control and proportional integral control," *Prz. Elektrotechniczny*, vol. 96, no. 10, pp. 156–162, 2020, doi: 10.15199/48.2020.10.29.

[25] M. Saeedifard, "Space Vector Modulation of Multi-Level and Multi-Module Converters for High Power Applications," Thèse de doctorat, Université de Toronto, 2008.

[26] C. A. C. Cavaliere, E. H. Watanabe, and M. Aredes, "Multi-pulse STATCOM operation under unbalanced voltages," *Proc. IEEE Power Eng. Soc. Transm. Distrib. Conf.*, vol. 1, no. c, pp. 567–572, 2002, doi: 10.1109/pesw.2002.985066.

[27] T. M. Blooming and D. J. Carnovale, "Application of IEEE STD 519-1992 harmonic limits," *Conf. Rec. 2006 Annu. Pulp Pap. Ind. Tech. Conf. IEEE*, pp. 1–9, 2006.